Fracture of bio-cemented sands

Charalampos Konstantinou[a], Emilio Martínez-Pañeda[b,1,*], Giovanna Biscontin[c], Norman A. Fleck[c]

[a]*Department of Civil and Environmental Engineering, University of Cyprus, 1678 Nicosia, Cyprus*
[b]*Department of Civil and Environmental Engineering, Imperial College London, London SW7 2AZ, UK*
[c]*Department of Engineering, Cambridge University, CB2 1PZ Cambridge, UK*
[d]*Department of Engineering Science, University of Oxford, Oxford OX1 3PJ, UK*

Abstract

Bio-chemical reactions enable the production of biomimetic materials such as sandstones. In the present study, microbiologically-induced calcium carbonate precipitation (MICP) is used to manufacture laboratory-scale specimens for fracture toughness measurement. The mode I and mixed-mode fracture toughnesses are measured as a function of cementation, and are correlated with strength, permeability and porosity. A micromechanical model is developed to predict the dependence of mode I fracture toughness upon the degree of cementation. In addition, the role of the crack tip T-stress in dictating kink angle and toughness is determined for mixed mode loading. At a sufficiently low degree of cementation, the zone of microcracking in the vicinity of the crack tip is sufficiently large for a crack tip K-field to cease to exist and for crack kinking theory to not apply. The interplay between cementation and fracture properties of sedimentary rocks is explained; this understanding underpins a wide range of rock fracture phenomena including hydraulic fracture.

Keywords:

Bio-cementation, Fracture, Cemented sands, bio-mediated materials, microbiologically-induced calcium carbonate precipitation

1. Introduction

There is a growing interest in using our understanding of the natural environment to inspire the invention of new materials and thereby expand material property space [1, 2]. This includes the development of *bio-mimetic* materials [3, 4], and the use of naturally occurring bio-chemical

---

*Corresponding author.
Email address: e.martinez-paneda@imperial.ac.uk (Emilio Martínez-Pañeda)

processes to create *bio-mediated* materials with unique properties [5]. Bio-cementation techniques have emerged as an environmentally-friendly approach to increase the strength of soils [6], heal cracks in concrete [7], and manufacture low-carbon building materials [8]. Among existing bio-cementation techniques, microbiologically induced calcium carbonate precipitation (MICP) has attracted particular attention for its ability to control the degree of cementation in the production of bio-cemented sands that mimic natural sandstones [9].

MICP involves the distribution and settlement of urease-producing bacteria within a granular matrix, see Fig. 1. First, a suspension of bacteria are introduced into the medium. The bacteria settle near the contact points between sand particles, and the cementation liquid is introduced repeatedly to generate calcium carbonate that binds the particles together. The cementation liquid consists of urea and a calcium source, usually calcium chloride. Calcium cations are attracted to the negatively charged cell walls of the bacteria and the microbes hydrolise urea to produce carbonate anions. Calcium carbonate precipitates on the bacterial wall, and consequently the position of the calcium carbonate crystals within the granular medium coincides with the location of the bacterial cells at contact points between the particles of a fine-grained sand [10]. The mass of cement between particles correlates with the concentration of cementation solution and this provides a means of generating specimens with selected levels of cementation. The above strategy has recently been exploited in studies on the tensile and compressive strength of artificial bio-mediated sandstones [11–14], and was linked to the microscale response either via SEM or via acoustic emissions [15], providing suitable grounds to develop simulation-based approaches based on discrete and lattice element methods [16–20]. However, the fracture behaviour of bio-cemented sands remains unexplored despite its importance to phenomena such as hydraulic fracture, groundwater decontamination and grouting.

In the current study the fracture of artificially bio-cemented sandstones is investigated by combining experiment and modelling. The mode I and mixed-mode fracture responses are measured and are correlated with permeability, porosity, and tensile and compressive strengths of samples that have been manufactured using the same MICP recipe. The crack path under mixed-mode macroscopic loading is quantified, including the sensitivity of kink angle to the T-stress of the crack tip stress field. Test methods are detailed in Section 2, and the experimental and modelling

results are given in Section 3. A micromechanical model is developed to predict the dependence of toughness upon the degree of cementation (Section 4). Concluding remarks are reported in Section 5.
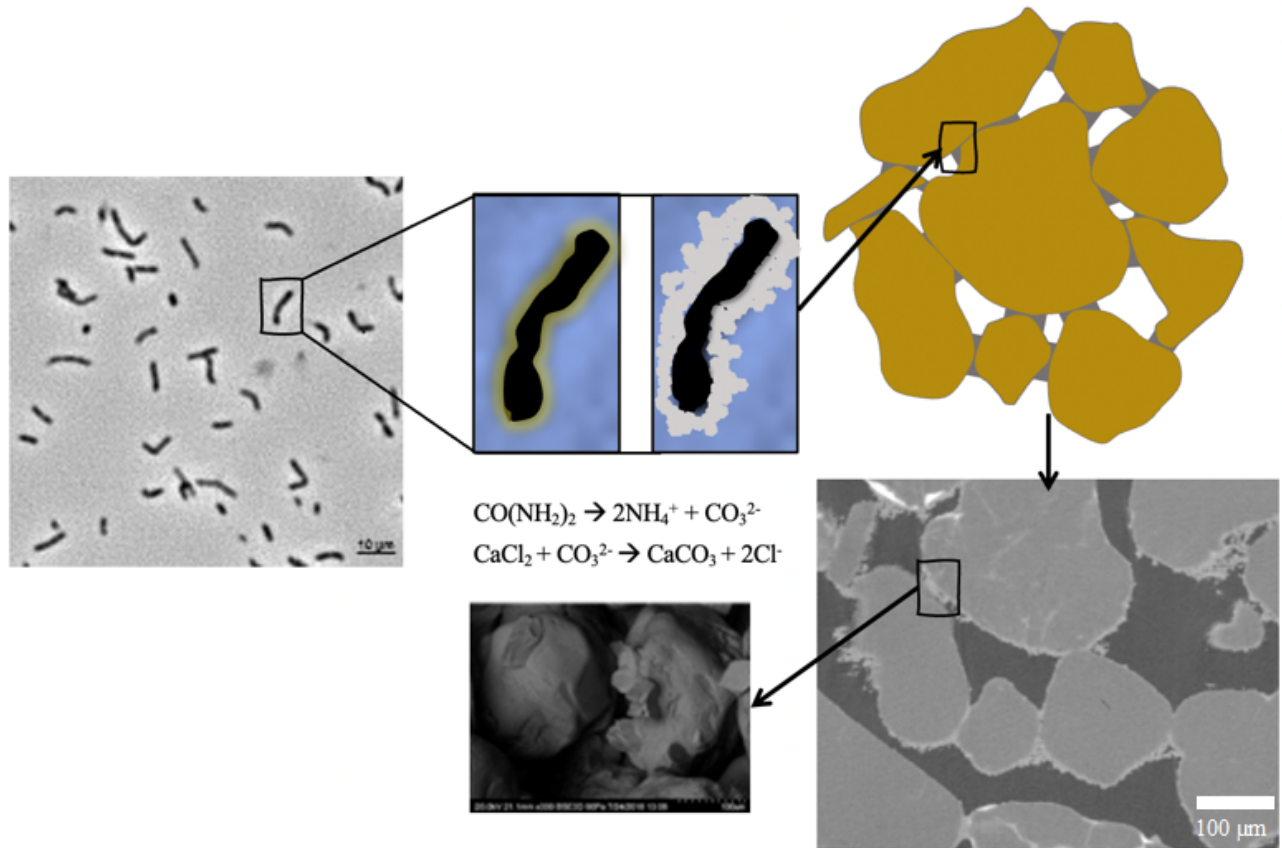

Figure 1: The use of bacteria to fabricate cemented sands. A sketch of microbially-induced calcium carbonate precipitation (MICP).

2. Experiments

The experimental protocol is now outlined, including the MICP parameters, sample preparation, and tests to measure mode I and mixed-mode fracture, permeability, porosity and bulk material strength (tensile and compressive). Silica sand was subjected to the MICP treatment; it comprised rounded to sub-rounded particles (medium sphericity) and a representative diameter (D_{90}) of 0.3 mm. The uniformity coefficient D_{60}/D_{10} was 1.38, thereby classifying the granular medium as poorly graded (uniform distribution of particles). Cylindrical samples of diameter 70 mm and height 150 mm were first prepared, and then cut into smaller test coupons. Previous compressive strength measurements have shown good reproducibility but it should be noted that

the scatter of the data increases with decreasing cementation level [9].

2.1. MICP parameters

MICP allows for control of the degree of cementation and thereby the macroscopic mechanical properties. The treatment involved the sequential injection of the bacterial solution (BS) and the cementation solution (CS), as explained in the Introduction.

(i) The bacterium *Sporosarcina pasteurii* was used as its urease-synthesis behaviour can be controlled in a relatively straightforward manner. The growth medium comprised 20 g/L yeast extract, 10 g/L ammonium sulphate, 20 g/L agar, and 0.13 M tris buffer. After 24 h of incubation at 30 °C, the culture was harvested and stored at 4 °C. The culture was introduced into liquid nutrient broth without agar, and placed in a shaking incubator for an additional 24 h to form the bacterial solution (BS); the BS was then introduced into sand columns. The optical density (OD), measured at a wavelength of 600 nm, OD_{600}, was between 1.5 and 2.0; the average urease activity was 0.8 (mM urea/h)/OD, as measured by a conductivity assay on a BS diluted to an OD of 1.0 [21].

(ii) The cementation solution (CS) consisted of 0.375 M urea, 0.25 M calcium chloride ($CaCl_2$), and 3 g/L nutrient broth. Previous studies have shown that this recipe gives an effective MICP treatment [22]. The combination of MICP parameters resulted in a uniform distribution of bacteria and chemicals without clogging. The rate of flow by gravity injection is balanced by the rate of MICP reaction, due to the chosen urease activity and concentration of the cementation solution. The long retention times promoted the efficient formation of calcium carbonate.

2.2. Sample preparation and calcium carbonate content

The injection direction in the cylindrical specimens was from top to bottom to give gravity-assisted permeation, thereby achieving uniform samples relative to other methods such as pumping. Before each injection, the excess solution was allowed to drain while the sample remained saturated. The time between two subsequent injections, the so-called retention time, was 24 hours. The degree of cementation was controlled by the number of CS injections, as the amount of calcium carbonate precipitation increases with the concentration of cementation solution, see Ref. [9] for

additional details.

The calcium carbonate ($CaCO_3$) content was measured according to the standard ASTM D4373-21, as follows. 30 mL of hydrochloric acid (HCl) 2.5M was introduced into 30 g of a dried and ground sample in order to generate carbon dioxide gas. Specifically, the $CaCO_3$ reacts with HCl as follows:

$$CaCO_{3(s)} + 2HCl_{(aq)} \rightarrow CaCl_{2(aq)} + CO_{2(g)} + H_2O_{(l)} \tag{1}$$

The quantity of calcium carbonate was calculated by measuring the mass of carbon dioxide released. To do so, the carbon dioxide gas was released into a calcimeter chamber and the gas pressure was measured using a pressure gauge. The gas pressure is related to the released amount of $CO_{2(g)}$ and, from the stoichiomentry of the above reaction, the amount of calcium carbonate was calculated. The degree of cementation is reported as the mass fraction of $CaCO_3$.

Once the bio-cementation process had been completed, specimens of 70 mm diameter and 150 height were extracted from the molds. They were oven-dried at a temperature of 105°C to remove all excessive soluble salts. The specimens were then cut into disks and a notch was introduced using a small knife.

2.3. Fracture toughness tests

Three-point bend tests on semi-circular disks of radius $R = 70$ mm were conducted to determine the mixed mode I and II fracture toughness, see Fig. 2. The test procedure followed the ISRM standard for fracture toughness measurement [23]. The samples were loaded quasi-statically under displacement-control at a rate of 0.05 mm/min. An initial notch of normalised length $a/R = 0.4$ was introduced, either parallel or inclined at an angle α with respect to the loading direction to give Mode I and Mixed-mode loading, respectively. The notch inclination angle α was of magnitude 0°, 15°, 30°, 45°, and 60° in order to span a wide range of mixed-mode behaviours. The span length is $S/R = 1.6$. The mode I fracture toughness for the choice $\alpha = 0$ is estimated from the peak load P_{max} as

$$K_{Ic} = Y \frac{P_{max}\sqrt{\pi a}}{2Rt} \tag{2}$$

where t is the sample thickness and the calibration factor Y is given by

$$Y = -1.297 + 9.516 \frac{S}{2R} - \left(0.47 + 16.457 \frac{S}{2R}\right) \frac{a}{R} + \left(1.071 + 34.401 \frac{S}{2R}\right) \left(\frac{a}{R}\right)^2 \tag{3}$$

For mixed-mode loading, the mode I and mode II stress intensity factors K_I and K_{II}, respectively, are related to the applied load P by

$$K_I = \frac{P\sqrt{\pi a}}{2Rt} Y_I\left(\alpha, \frac{a}{R}, \frac{S}{R}\right) \qquad \text{and} \qquad K_{II} = \frac{P\sqrt{\pi a}}{2Rt} Y_{II}\left(\alpha, \frac{a}{R}, \frac{S}{R}\right) \tag{4}$$

where the geometry factors Y_I and Y_{II} have already been obtained as a function of α, a/R, and S/R using finite element analysis [24]. Similarly, the elastic T-stress [25] is given by

$$T = \frac{P}{2Rt} Y_T\left(\alpha, \frac{a}{R}, \frac{S}{R}\right) \tag{5}$$

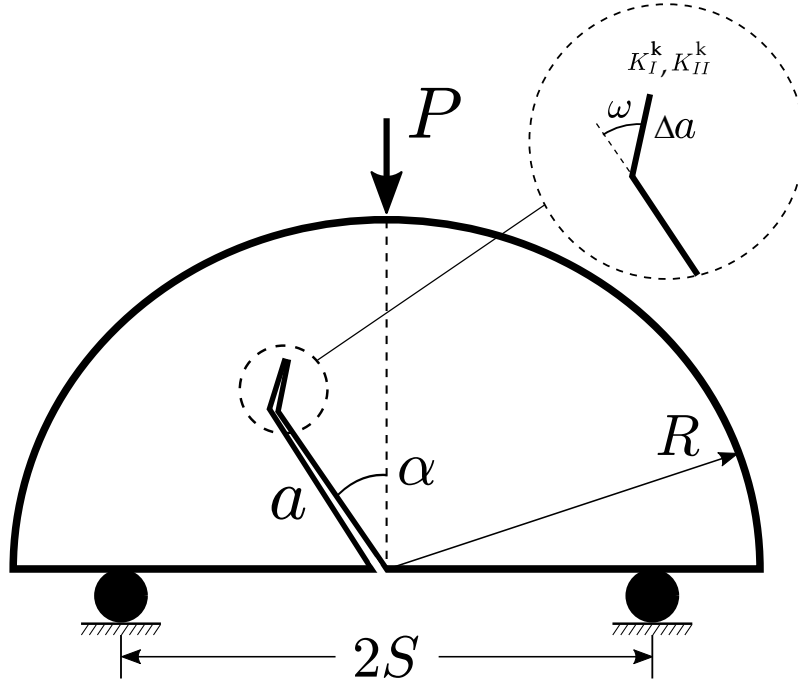where the calibration function Y_T has alrady been reported in Ref. [24].

Figure 2: The configuration of the mixed-mode fracture experiments, including the kink crack extension Δa and kink angle ω.

2.4. Relevant material properties

Fracture toughness measurements were complemented by experiments aimed at correlating the degree of cementation of bio-cemented sands with relevant material properties: unconfined compressive strength (UCS), tensile strength, porosity, and permeability [9, 10, 14]. All tests were conducted on samples prepared using the same MICP protocol and over the same range of cementation ($CaCO_3$ mass fraction) as used for the fracture toughness measurements.

Uniaxial compression tests were conducted on cylindrical samples by compressing them in the axial direction, in accordance with the standard ASTM D7012-14. The samples had a diameter of 70 mm and height of 150 mm, and the applied loading rate was 1.14 mm/min. The tensile strength was measured by means of the so-called Brazilian or indirect splitting test [26], using disk samples of diameter 70 mm and thickness 30 mm, in accordance with the standard ASTM D2936. The relationship between porosity p and $CaCO_3$ mass fraction was obtained from the bulk dry density ρ by using the usual relation:

$$p = 1 - \frac{\rho}{\rho_s} \tag{6}$$

where ρ_s is the weighted average density of silica and $CaCO_3$ [9]. The permeability was measured by falling head tests, using the injection molds as rigid wall permeameters after all excess soluble salts had been removed by flushing with de-ionised water.

3. Results

3.1. Mode I fracture

The dependence of mode I fracture toughness K_{Ic} upon mass fraction $\bar{m}$ of $CaCO_3$ is given in Fig.3a, while the tensile strength σ_f^t and compressive strength σ_f^c are plotted as a function of mass fraction $\bar{m}$ in Fig. 3b. Note that both K_{Ic} and σ_f^t increase almost linearly with $\bar{m}$ whereas σ_f^c scales with $\bar{m}$ in a non-linear fashion, consistent with the literature [27]. As the degree of cementation increases, such that $\bar{m}$ increases, the porosity and permeability both decrease, see Fig. 3c. This behaviour is consistent with the notion that cementation fills pore space and leads to a drop in permeability and to an increase in both macroscopic strength and fracture toughness. The range of porosities measured (0.32 to 0.37) is close to that exhibited by weak natural sandstones. A similar toughness-porosity relationship has been reported for sintered steels [28, 29] due to the feature-in-common that discrete necks exist between particles.

It is expected that internal flaws exist in cemented rocks of characteristic length $2a_0$ (such as the diameter of a penny-shaped crack, or the length of a through-crack) which much exceeds the particle diameter D. Consequently, the tensile strength σ_f^t is given by the criterion $K_I = \sigma_f^t \sqrt{\pi a_0} = K_{Ic}$ and the scatter in flaw size results in a scatter of tensile strength, as noted previously [14]. It is instructive to plot the measured tensile strength versus fracture toughness for the bio-cemented sand of the present study in Fig. 3d, and to include published data [30] for a range of cemented rocks. In

addition, we make use of the relation between tensile fracture strength σ_f^t and fracture toughness K_{Ic}, as given by $\sigma_f^t \sqrt{\pi a_0} = K_{Ic}$, to determine the critical defect size $a_0 = (1/\pi)(K_{Ic}/\sigma_f^t)^2$ that best fits the data. Taken together, the results show that bio-cemented sands have low values of both strength and fracture toughness relative to that of other rock-like materials. For the highest levels of cementation considered, bio-cemented sands can attain a tensile strength comparable to that of mudstone, but with a lower fracture toughness. The critical defect size a_0 that provides the best fit to the bio-cemented sands data decreases with increasing $\bar{m}$: low cemented bio-sands have critical defects as large as 5-10 mm, but as the degree of cementation increases a_0 is on the order of 1 mm. This is a smaller critical defect size than that of most rock-like materials and comparable to that of shale [31]. We note in passing that the defect size a_0 in the cemented bio-sands and in naturally occurring cemented rocks [30] is typically two orders of magnitude larger than the particle size D. Recall that the ASTM Standard E1820[1] demands that the crack length $a = 28$ mm in the test program must exceed $2.5(K_{Ic}/\sigma_f^t)^2 = 2.5\pi a_0$ in order for the test to give a valid measure of fracture toughness. Consequently, fracture toughness measurements based on a crack length of $a = 28$ mm are valid only for a_0 less than 3.5 mm. Thus, the K_{Ic} tests are valid for $\bar{m} \geq 5\%$ by making use of Figs. 3a, 3b and 3d. This raises the immediate question of whether the bio-cemented sand behaves in the manner of an elastic-brittle solid when subjected to mixed mode loading.

We further note that the critical defect size a_0 can be interpreted as the transition flaw size between strength-control and toughness-control. When a rock contains cracks much larger than a_0 its tensile strength is governed by its fracture toughness. In contrast, when small cracks are introduced (shorter than a_0), they have no effect upon the tensile strength of the rock as the tensile strength is set by the largest intrinsic flaw size of length a_0 [32].

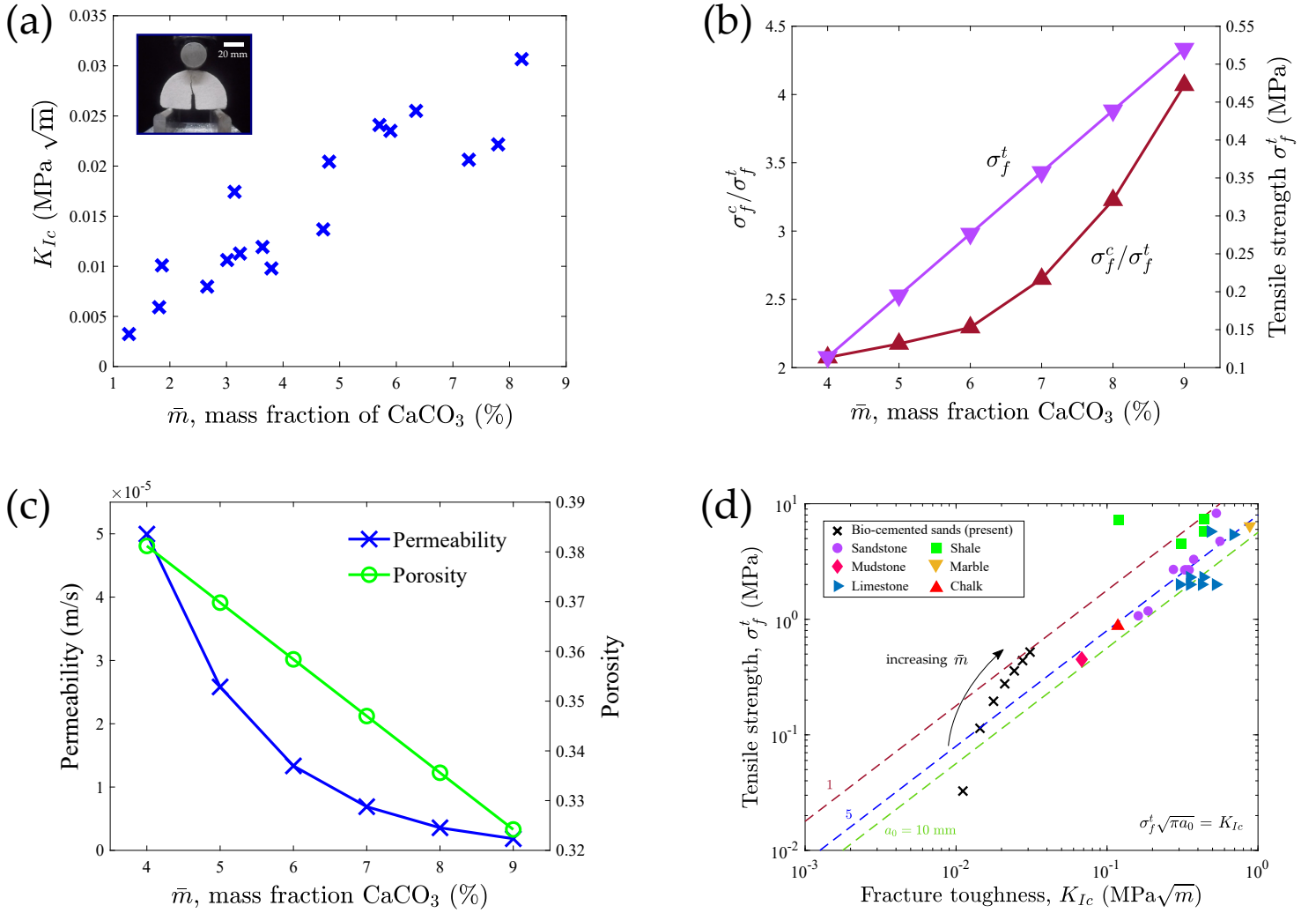[1]Standard Test Method for Measurement of Fracture Toughness

Figure 3: Experimental characterisation of the mechanical behaviour of bio-cemented sands: (a) Mode I fracture toughness K_{Ic}, (b) tensile strength σ_f^t and compressive strength σ_f^c as a function of cementation, (c) permeability and porosity as a function of cementation, and (d) correlation of tensile strength σ_f^t to fracture toughness for a range of cemented rocks.

3.2. Mixed-mode fracture

As shown in Fig. 2, the mixed mode experiments are conducted such that the initial crack is inclined at an angle α relative to the direction of applied load. Samples are produced for a wide range of α values and $CaCO_3$ mass fractions. The direction of crack growth is characterised by the so-called kink angle ω, see the inset of Fig. 2. The stress intensity factors that characterise the stress state at the tip of the kink crack (K_I^k, K_{II}^k) is related to the stress state at the tip of the original parent crack, as characterised by the stress intensity factors K_I and K_{II} [33]. The T-stress associated with the parent crack additionally contributes to the stress intensity at the tip of a kink crack of finite length Δa. Following He and Hutchinson [34] and He et al. [35], the stress

intensity factors at the tip of the kink crack are given by

$$K_I^k = A_I(\omega)K_I + B_I(\omega)K_{II} + C_I(\omega)T\sqrt{\Delta a} \qquad (7)$$

$$K_{II}^k = A_{II}(\omega)K_I + B_{II}(\omega)K_{II} + C_{II}(\omega)T\sqrt{\Delta a} \qquad (8)$$

where the coefficients A_i, B_i and C_i depend upon the kink angle ω and are provided in Refs. [34, 35].

The stress intensity factors (K_I, K_{II}) at the point of failure are determined from the critical applied load P, sample dimensions $(a/R, S/R)$ and initial crack angle α via Eq. (4). The locus of measured (K_I, K_{II}) at the initiation of crack growth is generated for selected values of α in Fig. 4a, for selected values of $CaCO_3$ mass fraction $\bar{m}$. Unstable fast fracture accompanies the initiation of crack growth for all crack lengths and crack orientations. The values of (K_I, K_{II}) are normalised by the mode I fracture toughness for each cementation level (as reported in Section 3.1). The failure locii in Fig. 4a are sensitive to the cementation level. This suggests that the damage zone is sufficiently large and diffuse at the point of instability that the initiation of crack growth cannot be reduced to the classical criterion of a critical value of K_I^k and $K_{II}^k = 0$ and $\Delta a = 0$, as commonly assumed as for crack tip kinking in brittle solids [36, 37]. However, in order to assess whether (7) and (8) can be used to reproduce the data of Fig. 4a, it is first necessary to determine an appropriate value of length Δa for the putative kink at the crack tip.

Our strategy is as follows. We determine a best-fitting value of Δa such that the predicted value of crack kink direction ω (such that $K_{II}^k = 0$) is in agreement with the observed value of kink angle, over the full range of values of initial crack angle α and cementation level $\bar{m}$. Then, with this value of Δa adopted as a material constant, the value of K_I^k is determined as a function of α and $\bar{m}$. Classical kinking theory suggests that K_I^k is invariant and equals the mode I fracture toughness of the solid, K_{IC}.
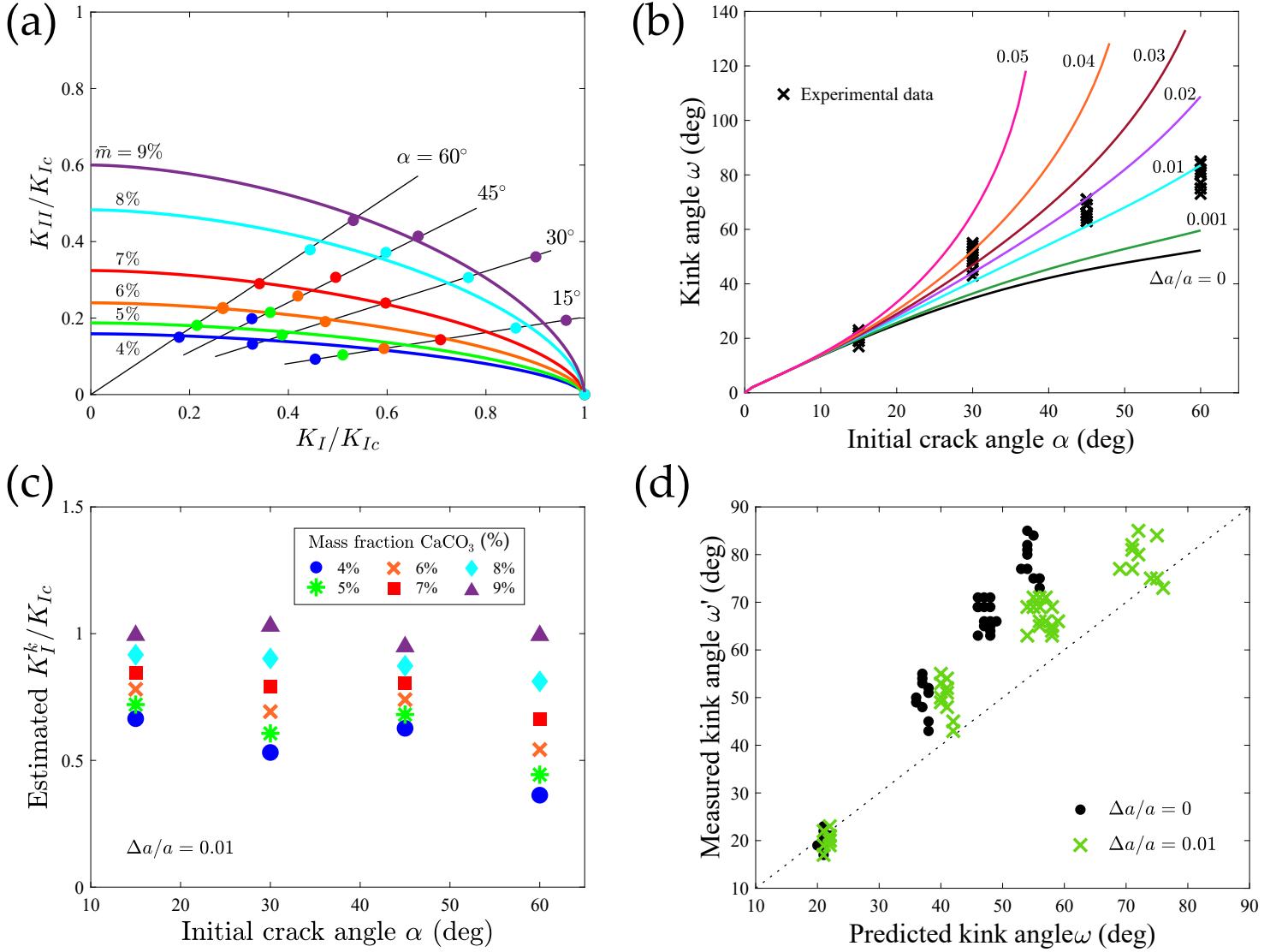
Figure 4: Mixed-mode fracture experiments: (a) critical stress intensity factors measured as a function of cementation ($\bar{m}$) and mode mixity (initial crack angle); (b) measured and predicted kink angles ω for the $K_{II}^k = 0$ criterion upon considering different values of the T-stress coefficient, as characterised by $\Delta a/a = 0.01$; (c) estimated values of K_I^k, normalised by K_{Ic}, for the choice of $\Delta a/a$ that provides the best fit to the measured kink angles; and (d) comparison between the measured and deduced kink angles for the choices $\Delta a = 0.01$ and $\Delta a = 0$, taking into account the role of the T-stress.

A *post-morten* examination of the samples was conducted to measure the sensitivity of observed kink angle ω to α and $\bar{m}$, see Fig. 4b. Predictions of ω are included by making use of Eq. (8) such that $K_{II}^k = 0$ for $a/R = 0.4$ and $S/R = 0.8$. The theoretical estimates are obtained for selected values of $\Delta a/a$ in order to assess the role of the T-stress. The choice $\Delta a/a = 0.01$ provides a good fit, and we note in passing that the choice $\Delta a/a = 0.01$ corresponds to $\Delta a = D$, where D is the particle diameter. This gives the putative crack length a clear physical interpretation

11

and lies within the regime of T-stress dominance [38]. The need to include the role of T-stress in the prediction of kink angle is emphasised in Fig. 4d: the assumption of a negligible T-stress, or equivalently the assumption that $\Delta a = 0$, underestimates the crack kinking angle as the degree of mode mix increases.

We proceed to use Eq. (7) to predict the value of K_I^k in each mixed-mode experiment, assuming that $(\Delta a/a = 0.01$, see Fig. 4b). The results given in Fig. 4c show that the inferred value of K_I^k is almost insensitive to the degree of mode mix. Further, the K_I^k values are close to the mode I fracture toughness at high $\bar{m}$ values. Some deviation is observed at low cementation levels, which is attributed to the diffuse nature of the cracking process [36, 37] and the similar size of the initial flaw and the transition flaw size of the material. The low sensitivity of the inferred K_I^k values to the degree of mode-mixity and their closeness to K_{Ic} (for high values of $\bar{m}$) suggest that elastic-brittle fracture mechanics and a local mode I kinking criterion are appropriate for bio-cemented sands, particularly at high cementation levels.

4. Discussion: A micromechanical model for particle fracture

A micromechanical model is now developed to predict the mode I fracture toughness of bio-mediated sandstones. Consider the idealised problem of a mode I K-field in the vicinity of the crack tip in a specimen that contains silica sand particles. The particles are treated as spheres of diameter D and are coated by a layer of $CaCO_3$ of thickness t_b, as shown in Fig. 5. The main purpose of the analysis is to develop scaling laws for fracture toughness and so the above idealisation of particle geometry is adequate for our purposes. Assume a simple cubic arrangement of sand particles, and restrict attention to a representative unit cell of side length D at the tip of a long crack. The tensile load on a crack tip particle is related to the macroscopic stress at that location σ^∞ according to

$$P = \frac{\pi D^2 \sigma^\infty}{4} \tag{9}$$

Write the radius of the bonded contact between particles as d and the average tensile stress acting over the bonded contact as σ_L, such that

$$P = \pi d^2 \sigma_L \tag{10}$$

Consequently, the local contact stress σ_L is related to the macroscopic stress σ^∞ by $\sigma_L = \left(D/2d\right)^2 \sigma^\infty$.

Recall that the dominant term in the series expansion of mode I crack tip stress at a distance r directly ahead of the crack tip is given by $\sigma = K_I/\sqrt{2\pi r}$. This stress field gives rise to the load P over the unit cell directly ahead of the crack tip, where

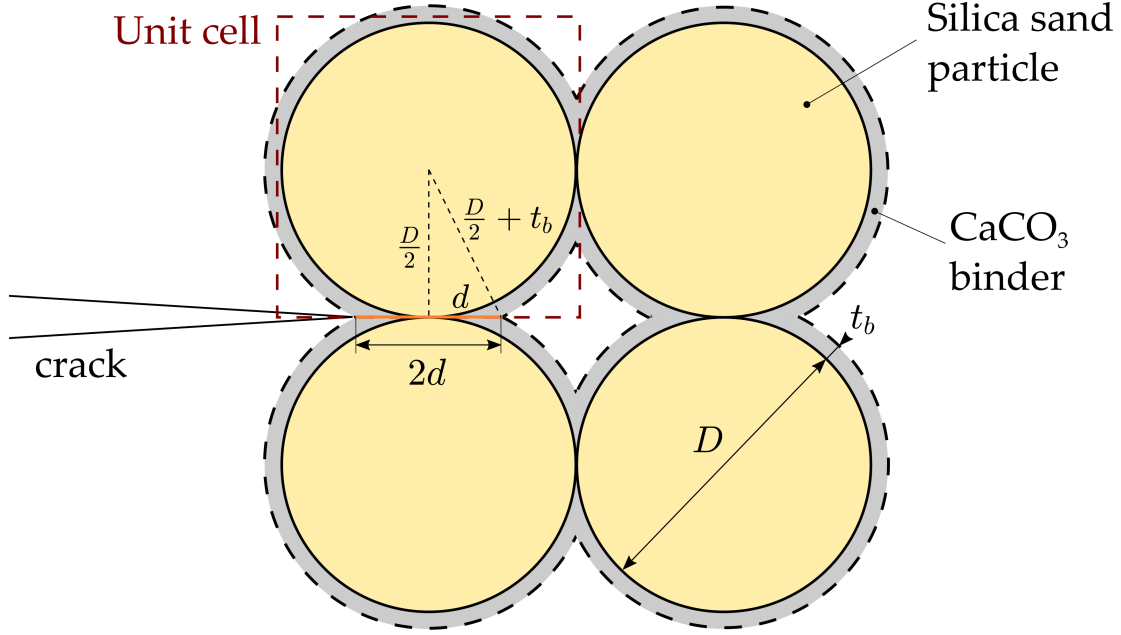$$P = \int_0^D \frac{K_I}{\sqrt{2\pi r}} D \, dr = \frac{2K_I D\sqrt{D}}{\sqrt{2\pi}} \tag{11}$$

Figure 5: A micromechanical description of fracture in bio-cemented sands. Silica sand particles of diameter D are surrounded by a thin layer of binder $CaCO_3$, of thickness t_b. The neck extends over a length $2d$.

Assume that crack advance occurs when the average contact stress σ_L at the neck immediately ahead of the crack tip attains the critical value σ_c. Then, the plane strain fracture toughness K_{Ic} follows from Eqs. (10) and (11) as

$$K_{Ic} = \frac{\pi^{3/2}}{\sqrt{2}} \left(\frac{d}{D}\right)^2 D^{1/2}\sigma_c \tag{12}$$

The mass fraction of binder is small and so the volume of binder can be approximated by $V_b \approx \pi D^2 t_b$, along with $d^2 \approx Dt_b$. Thus, the mass ratio $\bar{m}$ of binder to sand reads:

$$\bar{m} = \frac{\text{mass CaCO3}}{\text{mass silica}} = \frac{\rho_b}{\rho_s}\frac{6d^2}{D^2} \tag{13}$$

where the subscripts s and b denote sand and binder, respectively, and ρ denotes density. The above considerations suggest that the mode I fracture toughness scales with the degree of cementation,

and the tensile failure strength of the binder according to:

$$K_{Ic} = \frac{\pi^{3/2}}{\sqrt{2}} \frac{\bar{m}\rho_s}{6\rho_b} D^{1/2} \sigma_c \tag{14}$$

We proceed to investigate the ability of Eq. (14) to predict the sensitivity of fracture toughness to the degree of cementation. Assume that the density of silica sand and of $CaCO_3$ binder equals $\rho_s = 2.65$ Mg/m³ and $\rho_b = 2.71$ Mg/m³, respectively. The typical particle has a diameter of $D \equiv D_{90} = 0.3$ mm, and the local critical stress is taken to be $\sigma_c = 29$ MPa. Close agreement between the predictions of the model and experimental measurements is evident in Fig. 6, demonstrating the ability of the model to give the observed scaling of K_{Ic} with $CaCO_3$ mass fraction $\bar{m}$.
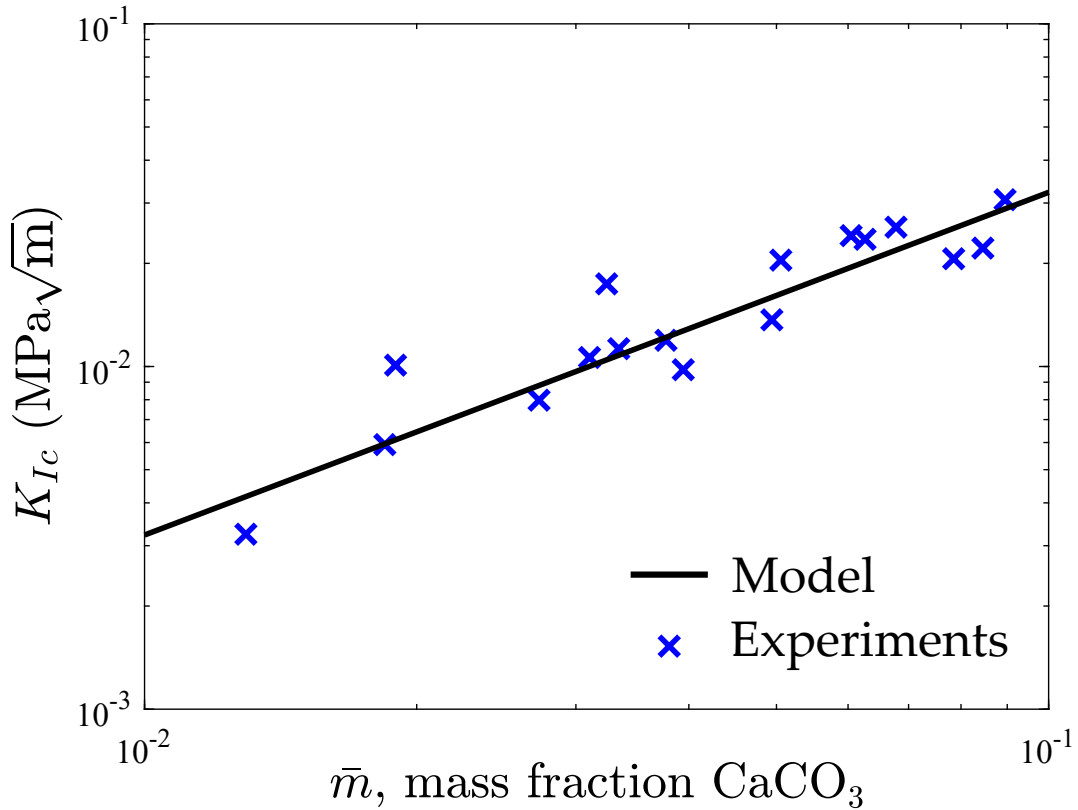

Figure 6: Micromechanical model predictions of fracture toughness K_{Ic} versus degree of cementation, as given by the mass fraction of $CaCO_3$.

5. Conclusions

We have used microbiologically induced calcium carbonate precipitation (MICP) to generate bio-treated sandstone-like materials with a controlled degree of cementation. This enables us to shed light on the interplay between cementation and relevant material properties (porosity, permeability, tensile and compressive strengths). Moreover, the relationship between cementation and

fracture behaviour is investigated. Mode I and mixed-mode fracture experiments are conducted and combined with theoretical analysis to gain mechanistic insight. A particle-level, micromechanical fracture model is developed to establish a correlation between the mode I fracture toughness K_{Ic} and the mass fraction $\bar{m}$ of CaCO$_3$. In addition, crack kinking theory is used to gain mechanistic insight into the role of T-stress upon the observed crack kinking angle. The main findings are:

- Fracture toughness, tensile strength and compressive strength increase with cementation, while permeability and porosity decrease. Porosity is the main source of defects and consequently the ratio of compressive to tensile strength decreases with decreasing cementation as a result of the associated increase in porosity.

- For the range of $\bar{m}$ values considered, bio-cemented sands exhibit low values of fracture toughness and strength relative to other rock-like materials, with only mudstones providing similar strengths. The critical defect size of the bio-cemented sands is $a_0 = 1$ mm, which is comparable to that of shale rock.

- The measured crack kinking angles increase with the degree of mode-mixity and can be adequately captured by including the role of the T-stress.

- The mode I kink tip fracture toughness K_I^k can be inferred from the mixed-mode experiments for all initial crack angles. At low cementation values, microcracking is more diffuse and linear elastic fracture mechanics does not apply for the specimen size adopted in the fracture tests.

- A micromechanical model for fracture toughness is supported by the experimental data, demonstrating its ability to capture the sensitivity of fracture toughness to the degree of cementation.

6. Acknowledgments

References

[1] S. Coyle, C. Majidi, P. LeDuc, K. J. Hsia, Bio-inspired soft robotics: Material selection, actuation, and design, Extreme Mechanics Letters 22 (2018) 51–59.

[2] F. Liu, T. Li, Z. Jia, L. Wang, Combination of stiffness, strength, and toughness in 3D printed interlocking nacre-like composites, Extreme Mechanics Letters 35 (2020) 100621.

[3] C. T. Bauer, E. Kroner, N. A. Fleck, E. Arzt, Hierarchical macroscopic fibrillar adhesives: In situ study of buckling and adhesion mechanisms on wavy substrates, Bioinspiration and Biomimetics 10 (6) (2015).

[4] D. Da, X. Qian, Fracture resistance design through biomimicry and topology optimization, Extreme Mechanics Letters 40 (2020) 100890.

[5] S. Deuerling, S. Kugler, M. Klotz, C. Zollfrank, D. Van Opdenbosch, A Perspective on Bio-Mediated Material Structuring, Advanced Materials 30 (19) (2018) 1–18.

[6] J. Chu, V. Stabnikov, V. Ivanov, Microbially Induced Calcium Carbonate Precipitation on Surface or in the Bulk of Soil, Geomicrobiology Journal 29 (6) (2012) 544–549.

[7] C. Lors, J. Ducasse-Lapeyrusse, R. Gagné, D. Damidot, Microbiologically induced calcium carbonate precipitation to repair microcracks remaining after autogenous healing of mortars, Construction and Building Materials 141 (2017) 461–469.

[8] D. M. Iqbal, L. S. Wong, S. Y. Kong, Bio-cementation in construction materials: A review, Materials 14 (9) (2021).

[9] C. Konstantinou, G. Biscontin, N. J. Jiang, K. Soga, Application of microbially induced carbonate precipitation to form bio-cemented artificial sandstone, Journal of Rock Mechanics and Geotechnical Engineering 13 (3) (2021) 579–592.

[10] C. Konstantinou, Y. Wang, G. Biscontin, K. Soga, The role of bacterial urease activity on the uniformity of carbonate precipitation profiles of bio-treated coarse sand specimens, Scientific Reports 11 (1) (2021) 1–17.

[11] K. Feng, B. M. Montoya, Influence of Confinement and Cementation Level on the Behavior of Microbial-Induced Calcite Precipitated Sands under Monotonic Drained Loading, Journal of Geotechnical and Geoenvironmental Engineering 142 (1) (2016) 1–9.

[12] M. J. Cui, J. J. Zheng, R. J. Zhang, H. J. Lai, J. Zhang, Influence of cementation level on the strength behaviour of bio-cemented sand, Acta Geotechnica 12 (5) (2017) 971–986.

[13] A. Nafisi, Elucidating the failure behavior and bond mechanics of bio-cemented sands, Ph.D. thesis, North Carolina State University (2019).

[14] C. Konstantinou, G. Biscontin, F. Logothetis, Tensile strength of artificially cemented sandstone generated via microbially induced carbonate precipitation, Materials 14 (16) (2021) 13–16.

[15] L. Wang, X. Jiang, X. He, J. Chu, Y. Xiao, H. Liu, E. K. Salje, Crackling noise and bio-cementation, Engineering Fracture Mechanics 247 (2021) 107675.

[16] P. A. Gago, C. Konstantinou, G. Biscontin, P. King, A numerical characterisation of unconfined strength of weakly consolidated granular packs and its effect on fluid-driven fracture behaviour, Rock Mechanics and Rock Engineering 55 (8) (2022) 4565–4575.

[17] L. Gong, L. Liu, Y. Xu, S. Zhu, T. Hao, A discrete element simulation considering calcite crystal shape to investigate the mechanical behaviors of bio-cemented sands, Construction and Building Materials 368 (2023) 130398.

[18] J. Shen, H. Wang, B. Zhou, G. Hu, X. Zhang, B. Yang, Investigation of the effect of microbial-induced calcite precipitation treatment on bio-cemented calcareous sands using discrete element method, Computers and Geotechnics 158 (2023) 105365.

[19] Z. Rizvi, Lattice element method and its application to multiphysics, Ph.D. thesis, Kiel University (2019).

[20] Z. H. Rizvi, M. Nikolić, F. Wuttke, Lattice element method for simulations of failure in bio-cemented sands, Granular matter 21 (2019) 1–14.

[21] V. S. Whiffin, Microbial CaCO3 precipitation for the production of biocement, Phd thesis, Murdoch University (2004).

[22] J. T. DeJong, M. B. Fritzges, K. Nüsslein, Microbially Induced Cementation to Control Sand Response to Undrained Shear, Journal of Geotechnical and Geoenvironmental Engineering 132 (11) (2006) 1381–1392.

[23] M. D. Kuruppu, Y. Obara, M. R. Ayatollahi, K. P. Chong, T. Funatsu, ISRM-suggested method for determining the mode i static fracture toughness using semi-circular bend specimen, Rock Mechanics and Rock Engineering 47 (1) (2014) 267–274.

[24] M. R. Ayatollahi, M. R. Aliha, Wide range data for crack tip parameters in two disc-type specimens under mixed mode loading, Computational Materials Science 38 (4) (2007) 660–670.

[25] C. Betegon, J. W. Hancock, Two-Parameter Characterization of Elastic-Plastic Crack-Tip Fields, Journal of Applied Mechanics 58 (1) (1991) 104–110.

[26] Y. Navidtehrani, C. Betegón, R. W. Zimmerman, E. Martínez-Pañeda, Griffith-based analysis of crack initiation location in a Brazilian test, International Journal of Rock Mechanics and Mining Sciences 159 (2022) 105227.

[27] D. Terzis, L. Laloui, 3-D micro-architecture and mechanical response of soil cemented via microbial-induced calcite precipitation, Scientific Reports 8 (1) (2018) 1–11.

[28] N. Fleck, R. Smith, Effect of density on tensile strength, fracture toughness, and fatigue crack propagation behaviour of sintered steel, Powder Metallurgy 3 (1981) 121–125.

[29] N. Fleck, R. Smith, Use of simple models to estimate the effect of density on fracture behaviour of sintered steel, Powder Metallurgy 3 (1981) 126–130.

[30] Ansys Granta EduPack, ANSYS Inc., Cambridge, UK, 2021.

[31] V. Kramarov, P. N. Parrikar, M. Mokhtari, Evaluation of Fracture Toughness of Sandstone and Shale Using Digital Image Correlation, Rock Mechanics and Rock Engineering 53 (9) (2020) 4231–4250.

[32] H. Gao, B. Ji, I. L. Jäger, E. Arzt, P. Fratzl, Materials become insensitive to flaws at nanoscale: lessons from nature, Proceedings of the national Academy of Sciences 100 (10) (2003) 5597–5600.

[33] J. L. Becker, R. M. Cannon, R. O. Ritchie, Finite crack kinking and T-stresses in functionally graded materials, International Journal of Solids and Structures 38 (32-33) (2001) 5545–5563.

[34] M. He, J. W. Hutchinson, Kinking of a Crack out of an Interface, Journal of Applied Mechanics 56 (1989) 270–278.

[35] M.-Y. He, A. Bartlett, A. Evans, J. W. Hutchinson, Kinking of a crack out of an interface role of inplane stress, Journal of the American Ceramic Society 74 (4) (1991) 767–771.

[36] Z. P. Bažant, B. H. Oh, Crack band theory for fracture of concrete, Materials and Structures 16 (3) (1983) 155–177.

[37] Z. P. Bažant, E. Becq-Giraudon, Statistical prediction of fracture parameters of concrete and implications for choice of testing standard, Cement and Concrete Research 32 (4) (2002) 529–556.

[38] L. Zhuo-Er, Y. Wei, An analytical solution to the stress fields of kinked cracks, Journal of the Mechanics and Physics of Solids 156 (2021) 104619.